

Phonon thermal transport shaped by strong spin-phonon scattering in a Kitaev material $\text{Na}_2\text{Co}_2\text{TeO}_6$

Xiaochen Hong^{1,2,*}, Matthias Gillig², Weiliang Yao³, Lukas Janssen^{4,†}, Vilmos Kocsis², Sebastian Gass², Yuan Li^{3,5}, Anja U. B. Wolter², Bernd Büchner^{2,6}, and Christian Hess^{1,2,‡}

¹*Fakultät für Mathematik und Naturwissenschaften,*

Bergische Universität Wuppertal, 42097 Wuppertal, Germany

²*Leibniz-Institute for Solid State and Materials Research (IFW-Dresden), 01069 Dresden, Germany*

³*International Center for Quantum Materials, School of Physics, Peking University, 100871 Beijing, China*

⁴*Institut für Theoretische Physik and Würzburg-Dresden Cluster of Excellence ct.qmat, Technische Universität Dresden, 01062 Dresden, Germany*

⁵*Collaborative Innovation Center of Quantum Matter, 100871 Beijing, China*

⁶*Institute of Solid State and Materials Physics and Würzburg-Dresden Cluster of Excellence ct.qmat, Technische Universität Dresden, 01062 Dresden, Germany*

The recent report of a half-quantized thermal Hall effect in the Kitaev material $\alpha\text{-RuCl}_3$ has sparked a strong debate on whether it is generated by Majorana fermion edge currents or whether other more conventional mechanisms involving magnons or phonons are at its origin. A more direct evidence for Majorana fermions which could be expected to arise from a contribution to the longitudinal heat conductivity κ_{xx} at $T \rightarrow 0$ is elusive due to a very complex magnetic field dependence of κ_{xx} . Here, we report very low temperature (below 1 K) thermal conductivity (κ) of another candidate Kitaev material, $\text{Na}_2\text{Co}_2\text{TeO}_6$. The application of a magnetic field along different principal axes of the crystal reveals a strong directional-dependent magnetic-field (\mathbf{B}) impact on κ . We show that no evidence for mobile quasiparticles except phonons can be concluded at any field from 0 T to the field polarized state. In particular, severely scattered phonon transport is observed across the $B - T$ phase diagram, which is attributed to prominent magnetic fluctuations. Cascades of phase transitions are uncovered for all \mathbf{B} directions by probing the strength of magnetic fluctuations via a precise record of $\kappa(B)$. Our results thus rule out recent proposals for itinerant magnetic excitations in $\text{Na}_2\text{Co}_2\text{TeO}_6$, and emphasise the importance of discriminating true spin liquid transport properties from scattered phonons in candidate materials.

Frustrated magnets refer to a set of materials that do not order down to temperatures well below the corresponding magnetic interaction strength. In some cases, the system is left with a ground state called quantum spin liquid (QSL), which is characterized by entangled spins, topological orders, and fractionalised magnetic excitations [1–3]. Kitaev QSL, proposed for bond-dependent nearest-neighbour interacting spins on the two-dimensional honeycomb lattice [4], is among the rare examples of exactly solvable QSL models [5–8]. Recent

research interest is further fueled by possible achieving Kitaev QSL in realistic materials. In particular, fingerprints of novel QSL-related excitations were revealed in $\alpha\text{-RuCl}_3$ [9, 10], both in its zero-field phase above the magnetic order [11], and more intriguingly, in its field-induced quantum disordered state [12].

However, those sought-after signatures for QSLs observed in $\alpha\text{-RuCl}_3$ always come along with alternative explanations. To be more specific on transport experiments, the report of half-integer quantization of thermal Hall conductance was once regarded as a definitive proof for the existence of Majorana fermions in the field-induced quantum disordered state in $\alpha\text{-RuCl}_3$ [12]. However, following experiments noticed such quantisation is less reproducible, and attributed the non-quantised temperature-dependent thermal Hall effect to phonons [13], or topological magnons [14]. On the other hand, quantum oscillations of longitudinal thermal conductivity in the quantum disordered state of $\alpha\text{-RuCl}_3$ suggest some fractionalised magnetic excitations forming a Fermi surface [15]. But such spectacle is also argued to be a result simply due to scattered phonons [13], in particular taking into account that no itinerant magnetic excitation has been found in a previous low temperature work [16]. On top of all these inconsistencies are the facts that $\alpha\text{-RuCl}_3$ suffers from the notorious stacking fault problem [17], from the dechlorination and oxidation after heat treatment [18], and more generally from sample dependence [19]. Thus, it is indispensable to seek for another example that can contribute to clarify to what extent these results are intrinsic to a Kitaev material.

In this paper, we studied the ground state properties of a quantum magnet $\text{Na}_2\text{Co}_2\text{TeO}_6$ (NCTO), which was recently investigated as a candidate Kitaev QSL [20–22], through the prism of low temperature thermal conductivity. Similar to its more famous cousin $\alpha\text{-RuCl}_3$, NCTO also features an intermediate quantum disordered phase sandwiched between the low field magnetically ordered state and the high-field polarized state [21, 22], where a QSL state is prospected. In this work, we report an anisotropic and astonishing large \mathbf{B} impact on κ at low temperatures (< 1 K). The analysis of our data

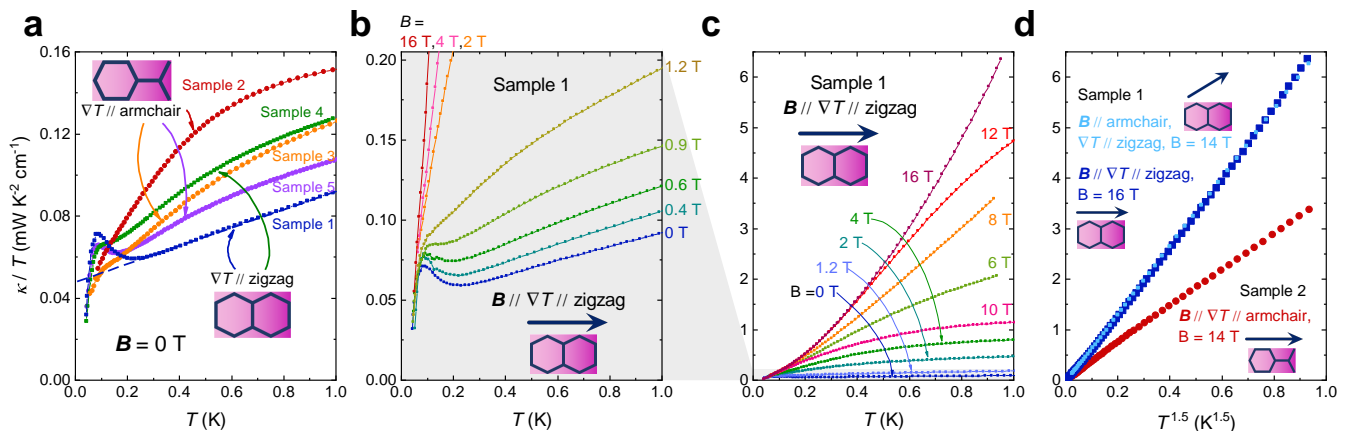


FIG. 1. **Thermal conductivity of $\text{Na}_2\text{Co}_2\text{TeO}_6$ and the impact of the in-plane magnetic fields.** **a**, In-plane thermal conductivity of five $\text{Na}_2\text{Co}_2\text{TeO}_6$ crystals without magnetic field. The thermal gradient (∇T) was set \parallel zigzag for Sample#1 and Sample#4, and \parallel armchair for the other three samples. By extrapolating the data to $T = 0$ K, a residual linear term ($\kappa/T|_{T \rightarrow 0}$) can be resolved for all five $\kappa/T(T)$ curves, especially clear for Sample#1, as indicated by the dashed blue line. **b**, The field dependence of the $\kappa/T(T)$ curves for Sample#1, focusing on the small field limit which covers a small portion of **c**, the full field dependence of the $\kappa/T(T)$ curves, as indicated by the gray background. At $T = 1$ K, the κ of Sample#1 experience a 70-fold increase from $B = 0$ T to the saturation field. **d**, The $\kappa/T(T)$ curves display a typical phononic $\propto T^\alpha$ behavior with $\alpha = 1.5$ at high enough fields. The field direction does not affect the saturated $\kappa/T(T)$ curves.

demonstrates that there is *no* evidence for mobile gapless QSL excitations (κ_{QSL}) contributing to κ . Instead, strongly scattered phonon transport (κ_{ph}), a quite traditional mechanism, is responsible for all the observed phenomena. Utilizing the high resolution $\kappa(B)$ data, we reveal a large density of magnetic excitations in the zero-field ground state of NCTO, further promoted excitations by magnetic field perpendicular to the honeycomb plane, and possible quantum criticality driven by in-plane magnetic field.

The residual linear term of thermal conductivity extrapolated to the low temperature limit ($\kappa_0/T \equiv \kappa/T|_{T \rightarrow 0}$) is persistently scrutinized for QSL candidates [3, 23], since its existence is practically regarded as a criterion for itinerant fractionalised magnetic excitations [24–28]. Fig. 1a shows κ/T of five NCTO crystals in zero magnetic field as a function of T . Albeit certain sample dependence, the $\kappa/T(T)$ profiles of all investigated crystals do not follow the simple power-law behavior expected for common insulators. Instead, regardless of the direction along which the thermal gradient ∇T is established (the two in-plane principal axes for the Co-honeycomb lattice, denoted as *zigzag* and *armchair* directions, indicated by the schematic insets), all $\kappa/T(T)$ profiles trend to end with a finite κ_0/T .

Among them, Sample#1 is especially notable for displaying a pronounced hump which emerges below about 250 mK. κ_0/T of Sample#1, extracted from a linear fit to its data above 250 mK, as highlighted by the dashed line in Fig. 1a, is $0.048 \text{ mW/K}^{-2}\text{cm}^{-1}$. At first glance, this finite κ_0/T is consistent with the notion that the ground state of NCTO is a QSL, since κ_{QSL} contributed by the putative fractionalized magnetic excitations is ex-

pected to scale linearly with T at the lowest temperatures [23]. We are aware of a recent work reporting similar data of NCTO, where these results have been interpreted as evidences for κ_{QSL} [29]. However, as clearly shown in Fig. 1a, the upturn of $\kappa/T(T)$ for Sample#1 (same for Sample#4 and Sample#5) terminates abruptly below about 100 mK, followed by a sharp drop, which results in a vanishing residual linear term that is incompatible with a gapless QSL ground state. Furthermore, we argue such observation is at odds with a hypothesised gapped QSL state with a gap size of the order ~ 100 mK. When a small in-plane magnetic field is applied, $\kappa_{QSL}/T(T)$ at temperatures below the initial gap energy scale is expected to increase due to a proliferation of quasiparticle excitations, while $\kappa/T(T)$ at higher temperatures should be less sensitive to the field since κ_{ph} is not directly affected. This is just opposite to our observations. As depicted in Fig. 1b, the field changes $\kappa/T(T)$ fundamentally above 100 mK, while it has basically no impact on the data at the lowest temperature.

Higher magnetic fields have a drastic impact on the $\kappa(T)/T$ curves until they finally saturate into a power-law behavior over the whole temperature range at the highest field. A representative case of Sample#1 is shown in Fig. 1c, along with the others displayed in Supp. Note 1 [30]. As can be seen in Fig. 1d, regardless of the (in-plane) field directions, $\kappa(T)/T$ curves for a given sample saturate at the same value.

Recent high-field magnetization experiments found the field-polarised state is reached for in-plane magnetic field higher than 10 T in NCTO [31]. As a result, spins can not contribute anymore, neither directly, nor indirectly through scattering at the highest field reached in this

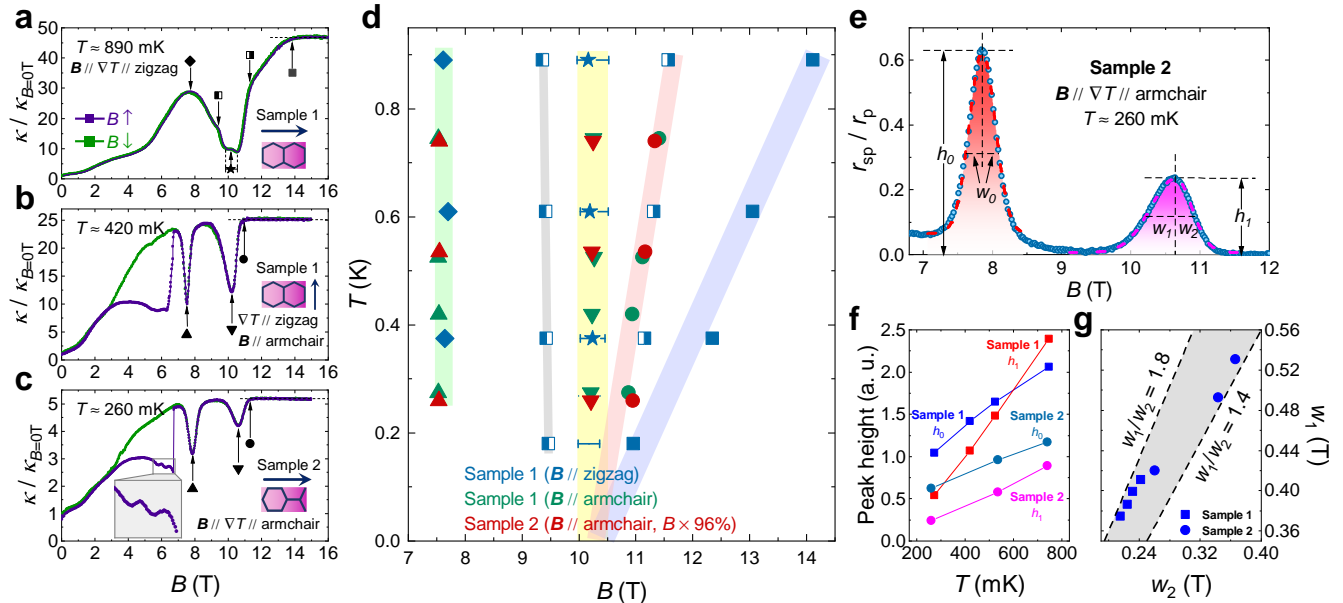


FIG. 2. **Anisotropic in-plane magnetic field effects on the thermal conductivity.** Panels **a**, **b**, and **c**, plot the normalized $\kappa(B)$ profiles of different combinations of $(\nabla T, B)$ orientations at selected temperatures. The purple curves and the green curves depict the data collected with field increasing and decreasing, respectively. All $\kappa(B)$ curves experience a saturation at high fields, signaling that a polarized state was reached in this study. Panels **a** and **b** depict the results of the same crystal (Sample#1) with the same ∇T orientation ($\nabla T \parallel \text{zigzag}$) but with different \mathbf{B} directions. They behave fundamentally different. Meanwhile Panel **b** resembles Panel **c** which is the data collected from another crystal (Sample#2) with a different ∇T orientation ($\nabla T \parallel \text{armchair}$) but the same field direction ($\mathbf{B} \parallel \text{armchair}$). As highlighted in the inset of Panel **c**, an oscillation-like feature can be distinguished before an abrupt increase of the $\kappa(B)$ for the field-up ramp. The anomalies in all $\kappa(T)$ curves are marked by different categories as glided by the background stripes. **d**, The temperature evolution of these anomalies of $\kappa(B)$ profiles. They are grouped into different categories as glided by the background stripes. The field values for Sample#2 are multiplied by 96%, in order to compromise the possible (out-of-plane) misalignment. **e**, A representative case of analysing the renormalized phonon-spin scattering strength (r_{sp}/r_p , see text). The peak at 7.5 T and 10.2 T (the field values for Sample#2 are multiplied by 96% as mentioned above) are fit to standard Gaussian function and skewed Gaussian function, respectively. The height and span of the peaks (h_0, w_0 for the 7.5 T peak, h_1, w_1 , and w_2 for the 10.2 T peak) are extracted as shown in the figure, and are summarized in Panel **f** and Panel **g**, respectively.

study. The saturated $\kappa(T)/T$ thus represents a standard ballistic phonon heat conductivity κ_{ph} in the low-temperature limit with $\kappa_{ph}/T \propto T^\alpha$, of which the exponent $\alpha = 1.5$. The sample independent $\alpha < 2$ indicates that the phonon reflection at the sample surface is not perfectly diffuse, and should be attributed to the intrinsic surface roughness of the as-grown NCTO crystals. One can thus take the $\kappa(T)/T$ curves at highest in-plane field as the intrinsic phonon thermal conductivity $\kappa_{ph}/T(T)$ free from the spin-phonon scattering.

As can be concluded from Fig. 1 and Supp. Fig. 1, there is no evidence for finite κ_0/T at any field. Furthermore, $\kappa/T(T)$ profiles at zero and low fields never exceed the saturated $\kappa_{ph}/T(T)$ over the whole temperature range. Hence, any evidence for a direct magnetic thermal transport channel on top of κ_{ph} , including κ_{QSL} , is elusive. If present, it must be negligibly small since the total measured κ at zero field is already at a very small value and at finite fields the saturated κ_{ph} is never exceeded. Hence, the intricate landscape of $\kappa(T)/T$ and its field dependence can be reasonably accounted for by

strong phonon-spin scattering, which is the main theme of the rest of the paper.

The field dependence of $\kappa/T(T)$ is non-monotonic, see Fig. 1c. A closer inspection can be performed by isothermal $\kappa/T(B)$ measurements. Fig. 2a-c exhibit the representative data of two samples with three different $(\nabla T, \mathbf{B})$ direction combinations. A straightforward conclusion is that $\kappa(B)$ is dictated by the \mathbf{B} direction, irrelevant to the ∇T direction. That further underlines the dominance of scattered κ_{ph} in NCTO over the whole field-temperature phase space. More specifically, a magnetic field applied along the *zigzag* and *armchair* directions on the same sample results in sharply different $\kappa(B)$ profiles. For $\mathbf{B} \parallel \text{zigzag}$ (Fig. 2a), there is strictly *no* hysteresis behavior. The overall feature turns out to be a broad dip centered around 10.2 T, with many minor anomalies marked by different symbols in the figure. For $\mathbf{B} \parallel \text{armchair}$ (Fig. 2b, Fig. 2c and Supp. Fig. 2e-2k), there are two very sharp dips at 7.5 T and 10.2 T. In contrast to the $\mathbf{B} \parallel \text{zigzag}$ case, a large hysteresis between 3 T and 6.5 T is evident. The abrupt increase of κ in

the up-ramp isotherm points to a first-order-like transition. Note that the \mathbf{B} direction dependent occurrence of hysteresis was already mentioned by higher temperature investigations [22, 32]. More discussion on the hysteretic behavior can be found in the Supp. Note 2 [30]. With both \mathbf{B} directions, κ saturates at high enough fields, as indicated by the dashed lines.

All the salient features in Fig. 2a-c and Supp. Fig. 2 are summarized in Fig. 2d. Beside the saturation field, which increases roughly linearly with temperature, the other anomalies are basically temperature independent. Such rich phase diagram suggests the landscape of successive \mathbf{B} induced phase transitions of the Heisenberg-Kitaev model might be inherited by NCTO [33]. Remarkably, three different finite-temperature anomalies marked by the yellow, red, and blue shaded areas seem to merge at around 10.2 T at 0 K, suggesting a quantum critical point. We expect the presented result to motivate further theoretical studies that account for specified parameters of NCTO in order to demystify these phases.

Some theoretical exploration on the Heisenberg-Kitaev honeycomb model have already revealed the potentially very rich phase diagram tuned by magnetic field [33]. Of particular interest is a multi-Q phase that can be stabilized in finite fields [33]. Recent experiments proposed the zero-field ground state of NCTO could be a triple-Q order [34–38], potentially stabilized by the proposed ring exchange interactions [36]. If confirmed, it could be a natural explanation of the extensive scattering of κ_{ph} at zero field, since a triple-Q ordered state guarantees larger density of state (DOS) of excitations around zero momentum (Γ point) which interact strongly with phonons [36]. These magnetic excitations should in principle contribute to specific heat. A decent experiment to exam this property is still pending for NCTO since heat capacity measurement at very low temperature is technically challenging [39]. Nevertheless, in Supp. Note 3 we argue our raw data can provide some indirect evidences for huge specific heat in the zero-field ground state [30]. Our data thus corroborate the notion of very large magnetic DOS as is expected for a triple-Q state.

Next we comment on the oscillation-like $\kappa(B)$ in the intermediate field range when $\mathbf{B} \parallel \textit{armchair}$, as highlighted in the inset of Fig. 2c. A similar feature exists but is less obvious in another sample and at higher temperatures, see Supp. Fig. 2g, 2h, and 2j [30]. Gapless QSL states that foster quantum oscillation of presumably charge neutral magnetic excitations are indeed anticipated for the Kitaev model [4, 40, 41], and was invoked to interpret the $\kappa(B)$ oscillations in $\alpha\text{-RuCl}_3$ [15]. Nevertheless, we believe quantum oscillations of κ_{QSL} should be irrelevant to NCTO. First of all, the oscillation feature in NCTO exists in the hysteresis region, thus in a magnetically ordered state. Besides, the fact that there is no evidence for itinerant κ_{QSL} at any field does not favor a quantum oscillation picture. Additionally, it is hard to imagine a significant direct contribution of κ_{QSL} which is exempted from the strong fluctuations that results in

a reduction of κ_{ph} by orders of magnitude. With this in mind, more caution should be taken for uniqueness of possible Kitaev QSL signatures observed in this material class, since thermal transport properties of NCTO share impressively similar features with $\alpha\text{-RuCl}_3$ [22, 42–44].

In view of the scattered phononic thermal conductivity has been revealed for NCTO, it is interesting to utilize the field evolution of κ/T as a natural probe for the phonon-spin scattering in this material [45, 46]. The relatively simple profiles of the $\mathbf{B} \parallel \textit{armchair}$ cases (Fig. 2b and 2c) allow a straightforward analysis. According to Matthiessen’s rule, the total phonon scattering rate is the sum of all independent ingredients, in this case the phonon-spin scattering (r_{sp}) and the intrinsic phononic scattering (r_p). At very low temperatures, r_p is determined only by the crystal size and is temperature independent because the phonon wave length diverges. It is the only scattering mechanism at play in the field polarized phase in the temperature range covered by this study. So the renormalized r_{sp}/r_p ($\equiv \kappa_{ph}/\kappa(B)-1$) is an index reflecting the magnetic scattering strength [46]. Fig. 2e exhibits one representative case for Sample#2 at about 260 mK. The $B = 7.5$ T peak is perfectly reproduced by a standard Gaussian distribution, which indicates randomly distributed disorder. However, the $B = 10.2$ T peak can only be reasonably fit by a skewed Gaussian distribution with different width at half maximum on both sides ($w_1 \neq w_2$). The extracted parameters are summarized in Fig. 2f and Fig. 2g. The fact that $w_1 > w_2$ might be key for identifying the actual type of phases surrounding the 10.2 T criticality, which needs material specific calculations to unravel.

Finally, at low temperatures, when \mathbf{B} is applied perpendicular to the NCTO honeycomb plane, κ gets further suppressed beyond a critical field of $B \approx 3$ T, as shown in Fig. 3a. In the language of magnetic scattering, it means the already strong magnetic fluctuations at zero field are even further promoted, contradictory to the intuition that field alignment of the magnetic moments should reduce them.

Indeed, there are some theoretical considerations predicting $\mathbf{B} \parallel c$ can lead to abundant phase transitions in the original Kitaev model and its variants [33, 40, 47–49]. Especially, quantum fluctuations in some of these intermediate phases are expected to be rather strong [49], in line with our observations that κ_{ph} gets further suppressed compared to the zero-field phase. As displayed more clearly in Fig. 3b, $\kappa/T(B)$ experiences a rapid drop between 2 T and 4 T. It is non-monotonic at higher field, featured by a broad hump around 8 T and a broad dip around 15 T, highlighted by the inset. We note the anomaly at about 15 T can be related to phase transitions revealed by a recent magnetization work [31], while the rapid drop between 2 T and 4 T do not have a similar correspondence.

To conclude, our high-quality low-temperature thermal transport study on NCTO single crystals established the dominance of phonon thermal transport in its magnetic

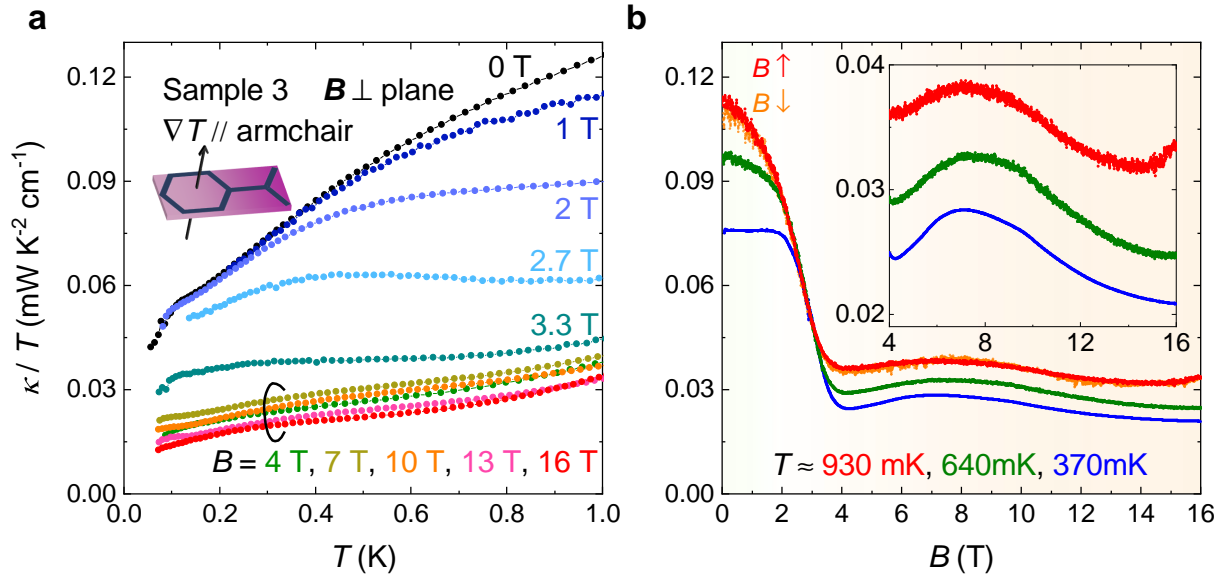


FIG. 3. **Further suppression of κ by out-of-plane magnetic fields.** **a**, The in-plane κ of Sample#3 under out-of-plane magnetic fields. The geometry is sketched in the inset. ∇T is along the *armchair* direction, and \mathbf{B} is perpendicular to the honeycomb plane. A rapid field suppression of κ/T is recognized at finite temperatures below about 3 T. At higher fields, the $\kappa/T(T)$ curves changes nonmonotonically in a narrow range. **b**, The $\kappa/T(B)$ profiles at three representative temperatures. They clearly show a fast drop at field $2 \text{ T} < B < 4 \text{ T}$, followed by an oscillation-like feature at higher fields. As highlighted in the inset, the oscillation profiles change little with temperature.

ground states, and exclude itinerant magnetic excitations of any form. The field evolution of κ , which manifests the strength of phonon-spin scattering, was taken as a probe to elucidate the intricate magnetic phases in NCTO. The strongly scattered phonons in the zero-field ground state indicates large DOS of magnetic excitations, in line with the proposal of a triple-Q state in NCTO. The in-plane κ depends significantly of the in-plane field direction, underlines the bond-dependent interactions of a Kitaev material. However, a criticality at 10.2 T is present regardless of the in-plane field direction. Field perpendicular to the honeycomb plane also induces multiple magnetic phases, where phonon-spin scattering is even more prominent than the zero-field phase. We expect similar physics should be quite common among QSL candidate materials, since QSLs are intrinsically at the edge of competing orders. The pervasive phase boundaries should be carefully considered when analysing existing and future experimental results of QSL candidate materials.

Methods

Sample preparation

Single crystals of $\text{Na}_2\text{Co}_2\text{TeO}_6$ were prepared with a modified flux method. Na_2CO_3 , Co_3O_4 and TeO_2 powders were grounded and loaded into an alumina crucible. Excess amount of TeO_2 served as a self-flux. The crucible was heated up to 1050°C , kept for two days, before cooling down to 600°C at a rate of 6.5°C per hour. Ruby-colored hexagonal flakes of typical size $\sim 10 \times 10 \times 0.1 \text{ mm}^3$ can be mechanically collected out of bluish violet residue. The harvested single crystals

were further washed with a NaOH solution. Basic characterizations of the as-grown crystals can be found in Ref [32].

The samples were cut into a size of about $\sim 5 \times 1 \times 0.1 \text{ mm}^3$, the longest direction along which ∇T was generated are the *armchair* or *zigzag* directions, respectively. In order to make thermal contacts to the fresh surface, the out-most layers of the as-grown crystals were cleaved off by a blade just before the silver paint was glued to it. As a result, the thickness of the samples were reduced to about $60 \mu\text{m}$.

Heat transport measurements

The thermal conductivities were measured in a dilution refrigerator, using a standard four-wire steady-state method with two RuO_2 chip thermometers, calibrated *in situ* against a reference RuO_2 thermometer. For fixed field $\kappa(T)$ measurements, each sample was initially cooled down from room temperature without magnetic field. The data were collected with gradually increased magnetic field in order to avoid the complicated situation of involving the hysteresis effect. $\kappa(T)$ data were collected in a steady-state manner (see Supp. Fig. 3 [30]).

To measure the $\kappa(B)$ isotherms, the system was cooled from the paramagnetic phase in zero field. Then the sample temperature was kept at a set point, and the field was changed from 0 T to the highest field (up-ramp), followed by decreasing to 0 T (down-ramp). The field was changed at a speed no more than 20 mT per minute, in order to minimize its heating effect, and to keep

the system in a (quasi-)thermal equilibrium state. In some cases, the field were ramped up and down multiple times, see Supp. Note 2 for more details [30].

We wish to point out that according to our experience, NCTO seems to have very strong anisotropic in-plane magnetic susceptibility at very low temperatures, that tend to align the *armchair* direction to the field. We are aware of a recently posted paper which reports a direct measurement of this magnetic anisotropy that underpins our conjecture [50]. In order to avoid experimental artifacts caused by such effect, the cooler side of all samples were glued to the heat sink (a gilded silver bulk) directly with a strong epoxy (Wakefield DeltaBond-152 two component adhesives). The samples

and the wires attached to them were checked carefully under a microscope after the experiments, to confirm they had not bent during the measurements.

Thermodynamic measurements

The magnetization measurements were carried out using a SQUID magnetometer (iHelium3, MPMS-XL, Quantum Design). The magnetostriction was measured using a commercially available dilatometer (Standard probe, Kuechler) compatible with the Quantum Design PPMS systems. These measurements are based on the capacitance measurement technique (AH2700A, Andeen-Hagerling).

-
- [1] Balents, L., Spin liquids in frustrated magnets. *Nature* **464**, 199–208 (2010). <https://doi.org/10.1038/nature08917>
- [2] Savary, L. & Balents, L., Quantum spin liquids: a review. *Rep. Prog. Phys.* **80**, 106502 (2017). DOI 10.1088/0034-4885/80/1/016502
- [3] Zhou, Y., Kanoda, K. & Ng, T.K. Quantum spin liquid states. *Rev. Mod. Phys.* **89**, 025003 (2017). <https://doi.org/10.1103/RevModPhys.89.025003>
- [4] Kitaev, A., Anyons in an exactly solved model and beyond. *Ann. Phys.* **321**, 2–111 (2006). <https://doi.org/10.1016/j.aop.2005.10.005>
- [5] Moessner, R., & Sondhi, S. L., Resonating Valence Bond Phase in the Triangular Lattice Quantum Dimer Model. *Phys. Rev. Lett.* **86**, 1881 (2001). <https://doi.org/10.1103/PhysRevLett.86.1881>
- [6] Wen, X.-G., Quantum Orders in an Exact Soluble Model. *Phys. Rev. Lett.* **90**, 016803 (2003). <https://doi.org/10.1103/PhysRevLett.90.016803>
- [7] Yao, H., Zhang, S.-C., & Kivelson, S. A., Algebraic Spin Liquid in an Exactly Solvable Spin Model. *Phys. Rev. Lett.* **102**, 217202 (2009). <https://doi.org/10.1103/PhysRevLett.102.217202>
- [8] Ben-Zion, D., Das, D., & McGreevy, J., Exactly solvable models of spin liquids with spinons, and of three-dimensional topological paramagnets. *Phys. Rev. B* **93**, 155147 (2016). <https://doi.org/10.1103/PhysRevB.93.155147>
- [9] Takagi, H., Takayama, T., Jackeli, G., Khaliullin, G. & Nagler, S. E. Concept and realization of Kitaev quantum spin liquids. *Nat. Rev. Phys.* **1**, 264–280 (2019). <https://doi.org/10.1038/s42254-019-0038-2>
- [10] Broholm, C., Cava, R. J., Kivelson, S. A., Nocera, D. G. Norman, M. R. & Senthil, T., Quantum spin liquids. *Science* **367**, 263 (2020). DOI: 10.1126/science.aay0668
- [11] Banerjee, A. *et al.*, Proximate Kitaev quantum spin liquid behavior in a honeycomb magnet. *Nat. Mat.* **15**, 733–740 (2016). <https://doi.org/10.1038/nmat4604>
- [12] Kasahara, Y. *et al.*, Majorana quantization and half-integer thermal quantum Hall effect in a Kitaev spin liquid. *Nature* **559**, 227–231 (2018). <https://doi.org/10.1038/s41586-018-0274-0>
- [13] Lefrançois, É., Baglo, J., Barthélemy, Q., Kim, S., Kim, Y.-J. & Taillefer, L., Oscillations in the magnetothermal conductivity of α -RuCl₃: Evidence of transition anomalies. *Phys. Rev. B* **107**, 064408 (2023). <https://doi.org/10.1103/PhysRevB.107.064408>
- [14] Czajka, P. *et al.*, Planar thermal Hall effect of topological bosons in the Kitaev magnet α -RuCl₃. *Nat. Mater.* **22**, 36–41 (2023). <https://doi.org/10.1038/s41563-022-01397-w>
- [15] Czajka, P. *et al.*, Oscillations of the thermal conductivity in the spin-liquid state of α -RuCl₃. *Nat. Phys.* **17**, 915–919 (2021). <https://doi.org/10.1038/s41567-021-01243-x>
- [16] Yu, Y.J. *et al.*, Ultralow-Temperature Thermal Conductivity of the Kitaev Honeycomb Magnet α -RuCl₃ across the Field-Induced Phase Transition. *Phys. Rev. Lett.* **120**, 067202 (2018). <https://doi.org/10.1103/PhysRevLett.120.067202>
- [17] Zhang, H. *et al.*, Stacking disorder and thermal transport properties of α -RuCl₃. *online preprint* arXiv:2303.03682
- [18] Breitner, F. A., Jesche, A., Tsurkan, A., & Gegenwart, P., Thermal decomposition of the Kitaev material α -RuCl₃ and its influence on low-temperature behavior. *online preprint* arXiv:2303.11308
- [19] Kasahara, Y. *et al.*, Quantized and unquantized thermal Hall conductance of the Kitaev spin liquid candidate α -RuCl₃. *Phys. Rev. B* **106**, L060410 (2022). <https://doi.org/10.1103/PhysRevB.106.L060410>
- [20] Liu, H. and & Khaliullin, G., Pseudospin exchange interactions in d^7 cobalt compounds: Possible realization of the Kitaev model. *Phys. Rev. B* **97**, 014407 (2018). <https://doi.org/10.1103/PhysRevB.97.014407>
- [21] Lin, G. *et al.*, Field-induced quantum spin disordered state in spin-1/2 honeycomb magnet Na₂Co₂TeO₆. *Nat. Commun.* **12**, 5559 (2021). <https://doi.org/10.1038/s41467-021-25567-7>
- [22] Hong, X. *et al.*, Strongly scattered phonon heat transport of the candidate Kitaev material Na₂Co₂TeO₆. *Phys. Rev. B* **104**, 144426 (2021). <https://doi.org/10.1103/PhysRevB.104.144426>
- [23] Yamashita, M., Shibauchi, T. & Matsuda, Y., Thermal-transport studies on two-dimensional quantum spin liquids. *Chemphyschem* **13**, 74–78 (2012). <https://doi.org/10.1002/cphc.201100556>
- [24] Yamashita, M. *et al.*, Highly Mobile Gapless Excitations in a Two-Dimensional Candidate Quantum Spin Liq-

- uid. *Science* **328**, 1246-1248 (2010). DOI: 10.1126/science.118820
- [25] Hartstein, M. *et al.*, Fermi surface in the absence of a Fermi liquid in the Kondo insulator SmB₆. *Nat. Phys.* **14**, 166–172 (2018). <https://doi.org/10.1038/nphys4295>
- [26] Li, N. *et al.*, Possible itinerant excitations and quantum spin state transitions in the effective spin-1/2 triangular-lattice antiferromagnet Na₂BaCo(PO₄)₂. *Nat. Commun.* **11**, 4216 (2020). <https://doi.org/10.1038/s41467-020-18041-3>
- [27] Sato, Y. *et al.*, Charge-neutral fermions and magnetic field-driven instability in insulating YbIr₃Si₇. *Nat. Commun.* **13**, 394 (2022). <https://doi.org/10.1038/s41467-021-27541-9>
- [28] Pan, B. *et al.*, Unambiguous Experimental Verification of Linear-in-Temperature Spinon Thermal Conductivity in an Antiferromagnetic Heisenberg Chain. *Phys. Rev. Lett.* **129**, 167201 (2022). <https://doi.org/10.1103/PhysRevLett.129.167201>
- [29] Guang, S. K. *et al.*, Thermal transport of fractionalized antiferromagnetic and field-induced states in the Kitaev material Na₂Co₂TeO₆. *Phys. Rev. B* **107**, 184423 (2023). <https://doi.org/10.1103/PhysRevB.107.184423>
- [30] Supplementary Materials attached at the end of this file
- [31] Zhang, S. *et al.*, Electronic and magnetic phase diagrams of Kitaev quantum spin liquid candidate Na₂Co₂TeO₆. *online preprint* arXiv:2212.03849
- [32] Yao, W. & Li, Y., Ferrimagnetism and anisotropic phase tunability by magnetic fields in Na₂Co₂TeO₆. *Phys. Rev. B* **101**, 085120 (2020). <https://doi.org/10.1103/PhysRevB.101.085120>
- [33] Janssen, L., Andrade, E. C. & Vojta, M., Honeycomb-Lattice Heisenberg-Kitaev Model in a Magnetic Field: Spin Canting, Metamagnetism, and Vortex Crystals. *Phys. Rev. Lett.* **117**, 277202 (2016). <https://doi.org/10.1103/PhysRevLett.117.277202>
- [34] Chen, W. *et al.*, Spin-orbit phase behavior of Na₂Co₂TeO₆ at low temperatures. *Phys. Rev. B* **103**, L180404 (2021). <https://doi.org/10.1103/PhysRevB.103.L180404>
- [35] Lee, C. H. *et al.*, Multistage development of anisotropic magnetic correlations in the Co-based honeycomb lattice Na₂Co₂TeO₆. *Phys. Rev. B* **103**, 214447 (2021). <https://doi.org/10.1103/PhysRevB.103.214447>
- [36] Krüger, W. G. F., Chen, W., Jin, X., Li, Y. & Janssen, L., Triple-Q order in Na₂Co₂TeO₆ from proximity to hidden-SU(2)-symmetric point. *online preprint* arXiv:2211.16957
- [37] Yao, W. *et al.*, Magnetic ground state of the Kitaev Na₂Co₂TeO₆ spin liquid candidate. *Phys. Rev. Research* **5**, L022045 (2023). <https://doi.org/10.1103/PhysRevResearch.5.L022045>
- [38] Kikuchi, J., Kamoda, T., Mera, N., Takahashi, Y., Okumura, K. & Yasui, Y., Field evolution of magnetic phases and spin dynamics in the honeycomb lattice magnet Na₂Co₂TeO₆: ²³Na NMR study. *Phys. Rev. B* **106**, 224416 (2022). <https://doi.org/10.1103/PhysRevB.106.224416>
- [39] Wilhelm, H., Lühmann, T., Rus, T., & Steglich, F., A compensated heat-pulse calorimeter for low temperatures. *Rev. Sci. Instrum.* **75**, 2700–270 (2004). <https://doi.org/10.1063/1.1771486>
- [40] Gohlke, M., Moessner, R. & Pollmann, F., Dynamical and topological properties of the Kitaev model in a [111] magnetic field. *Phys. Rev. B* **98**, 014418 (2018). <https://doi.org/10.1103/PhysRevB.98.014418>
- [41] Hickey, C. & Trebst, S., Emergence of a field-driven U(1) spin liquid in the Kitaev honeycomb model. *Nat. Commun.* **10**, 530 (2019). <https://doi.org/10.1038/s41467-019-08459-9>
- [42] Hentrich, R. *et al.*, Unusual phonon heat transport in α -RuCl₃: Strong spin-phonon scattering and field-induced spin gap. *Phys. Rev. Lett.* **120**, 117204 (2018). <https://doi.org/10.1103/PhysRevLett.120.117204>
- [43] Hentrich, R. *et al.*, Large thermal Hall effect in α -RuCl₃: Evidence for heat transport by Kitaev-Heisenberg paramagnons. *Phys. Rev. B* **99**, 085136 (2019). <https://doi.org/10.1103/PhysRevB.99.085136>
- [44] Gillig, M. *et al.*, Phononic-magnetic dichotomy of the thermal Hall effect in the Kitaev-Heisenberg candidate material Na₂Co₂TeO₆. *online preprint* arXiv:2303.03067
- [45] Gillig, M. *et al.*, Thermal transport of the frustrated spin-chain mineral linarite: Magnetic heat transport and strong spin-phonon scattering. *Phys. Rev. B* **104**, 235129 (2021). <https://doi.org/10.1103/PhysRevB.104.235129>
- [46] Hong, X. *et al.*, Heat transport of the kagome Heisenberg quantum spin liquid candidate YCu₃(OH)_{6.5}Br_{2.5}: Localized magnetic excitations and a putative spin gap. *Phys. Rev. B* **106**, L220406 (2022). <https://doi.org/10.1103/PhysRevB.106.L220406>
- [47] Sørensen, E. S., Catuneanu, A., Gordon, J. S. & Kee, H.-Y., Heart of Entanglement: Chiral, Nematic, and Incommensurate Phases in the Kitaev-Gamma Ladder in a Field. *Phys. Rev. X* **11**, 011013 (2021). <https://doi.org/10.1103/PhysRevX.11.011013>
- [48] Li, H. *et al.*, Identification of magnetic interactions and high-field quantum spin liquid in α -RuCl₃. *Nat. Commun.* **12**, 4007 (2021). <https://doi.org/10.1038/s41467-021-24257-8>
- [49] Chern, L. E., Kaneko, R., Lee, H.-Y. & Kim, Y. B., Magnetic field induced competing phases in spin-orbital entangled Kitaev magnets. *Phys. Rev. Research* **2**, 013014 (2020). <https://doi.org/10.1103/PhysRevResearch.2.013014>
- [50] Lin, G. *et al.*, Evidence for field induced quantum spin liquid behavior in a spin-1/2 honeycomb magnet. *online preprint at Research Square* <https://doi.org/10.21203/rs.3.rs-2034295/v1>

* * *

Corresponding author email:
 *xhong@uni-wuppertal.de
 †lukas.janssen@tu-dresden.de
 ‡c.hess@uni-wuppertal.de

Acknowledgements

We thank Jeroen van den Brink, Matthias Vojta, Vladislav Kataev, Christoph Wellm, Satoshi Nishimoto, Wenjie Chen, Yang Xu, and Wilhelm Krüger for illuminating discussions and collaboration on related work. We would like to thank Nicolás Pérez for generously sharing the equipment, and thank Danny Baumann and Tino

Schreiner for their technical assistance, especially during the pandemic lab-shutdown crisis.

Funding Acknowledgement:

This work has been supported by the Deutsche Forschungsgemeinschaft (DFG) through SFB 1143 (Project-ID No.247310070) and the Würzburg-Dresden Cluster of Excellence *ct.qmat* (EXC 2147, Project-ID No. 390858490).

C.H. has received funding from the European Research Council (ERC) under the European Union's-Horizon 2020 research and innovation programme (Grant Agreement No. 647276-MARS-ERC-2014-CoG).

L.J. was supported by the DFG through the Emmy Noether program (JA2306/4-1, Project No. 411750675).

V.K. was supported by the Alexander von Humboldt Foundation.

Y.L. acknowledges funding support from the National Basic Research Program of China (Grant No.

2021YFA1401901) and the NSF of China (Grant No. 12061131004).

Author contributions

B.B., C.H., and Y.L. conceived and initiated the study. W.Y. and Y.L. grown the crystals. X.H. and M.G. performed the transport measurements. V.K., S.G., and A.U.B.W. performed the thermodynamic measurements. X.H., C.H., and L.J. analysed the data. X.H., C.H., L.J., and V.K. wrote the manuscript with input from all authors. C.H. supervised the project.

Additional Information

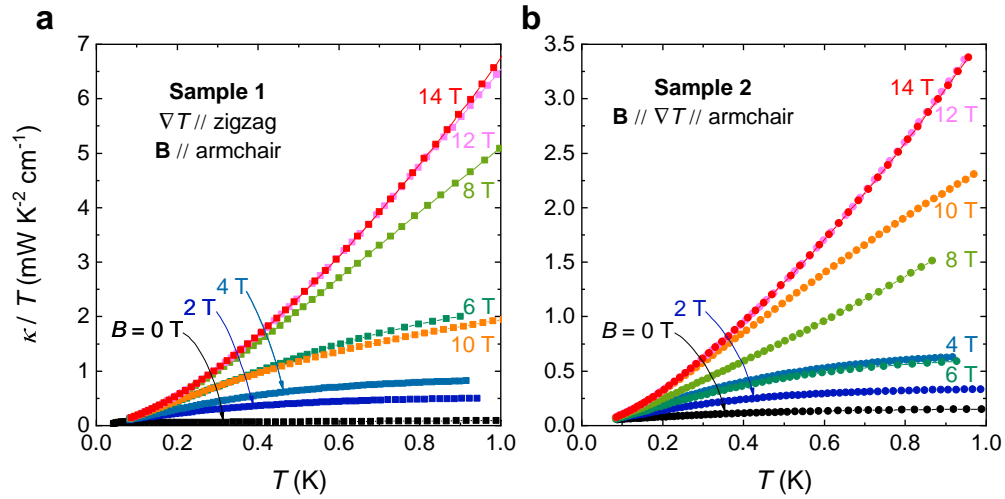
Supplementary information is available at the end of the paper.

Competing financial interests

The authors declare no competing financial interests.

Supplementary Materials for:
**Phonon thermal transport shaped by strong spin-phonon scattering
 in a Kitaev material $\text{Na}_2\text{Co}_2\text{TeO}_6$**

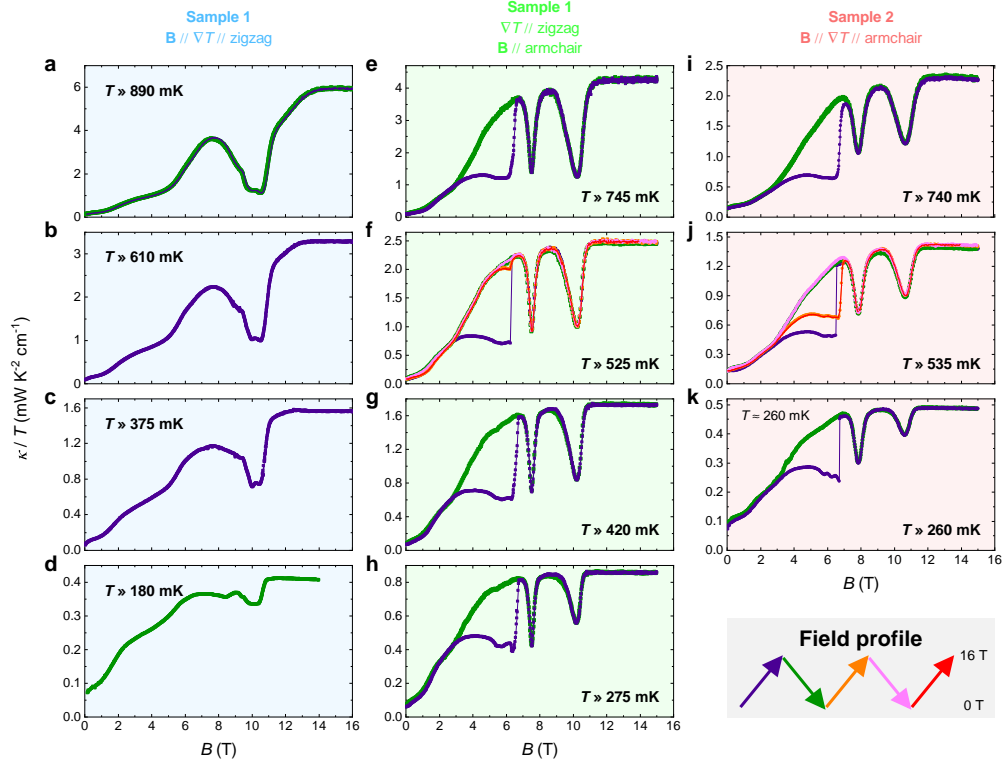
Supplementary Note 1: Additional $\kappa/T(T)$ data.



Supplementary Figure 1 | The $\kappa/T(T)$ curves of two samples with field applied along the *armchair* direction. **a**, Sample#1. **b**, Sample#2.

Supplementary Fig. 1 shows the field dependent $\kappa/T(T)$ curves of two crystals, for $\mathbf{B} // \textit{armchair}$ direction. They have similar behavior as the results shown in Fig. 1c of the main text, in that field increases κ non-monotonically, until it reaches the saturation field. The data of Sample#1 (Supp. Fig. 1a) was collected on the same sample measured for Fig. 1c with intact thermal contacts. Only the magnetic field direction is rotated from the *zigzag* direction to the *armchair* direction.

Supplementary Note 2: Additional $\kappa/T(B)$ data and discussion on the hysteresis behavior.



Supplementary Figure 2 | The $\kappa/T(B)$ isotherms with different combinations of $(\nabla T, B)$ orientations. Different background colour stands for different $(\nabla T, B)$ orientations as specified on the top of the panels. The data in the blue column (a - d) and the green column (e - h) were collected on the same crystal after reorienting the field direction. The gray box at the right-bottom corner depicts how the field was applied, at each fixed temperature, after zero field cooling from the paramagnetic higher temperature phase. The data are plotted in violet for the first up-field ramp. Before warming up above 1 K, the second ramp from high field to zero field was plotted in olive, followed by the orange (ramp up), magenta (ramp down), and the red (ramp up) curves.

As shown in Supplementary Fig. 2a, we cannot resolve any hysteresis for \mathbf{B} applied along

the *zigzag* direction.

When \mathbf{B} is applied along the *armchair* direction, the hysteresis behavior is evident between 3 T to 6.5 T. Magnetic field was ramped up and down at selected temperatures (Supp. Fig. 2f and 2j) for both samples. In both cases, one can see the second up-ramp $\kappa/T(B)$ curve after the saturation field has been reached is different from the first up-ramp $\kappa/T(B)$ curve, but overlaps with the third up-ramp $\kappa/T(B)$ curve. The down-ramp $\kappa/T(B)$ curves are never affected. Obviously, a field hysteresis and the sudden jump of κ for the up-field ramp at around 6.5 T point to a first-order transition with a large energy barrier between the two valleys of the energy landscape. We propose two possible mechanisms that can lead to such observation:

Scenario A: The magnetically ordered phases of NCTO are different in the low ($\mathbf{B}_{\parallel armchair} < 3$ T) field region and the higher ($\mathbf{B}_{\parallel armchair} > 6.5$ T) field region, and mix in the intermediate field range of 3 T $< \mathbf{B}_{\parallel armchair} < 6.5$ T. The corresponding states have different excitation DOS at (small) finite temperatures, which induce different phonon scattering strengths. These two states are separated by a large energy barrier. In the field range of 3 T $< \mathbf{B}_{\parallel armchair} < 6.5$ T, both states are locally stable. During the first up-field ramp, the system is distributed into the two states according to their energy landscape. Applying field $\mathbf{B} \parallel armchair$ helps to populate the state with lower DOS. The dominance of the lower DOS state prevails until the system enters the $\mathbf{B}_{\parallel armchair} < 3$ T state again in the down-field ramp. However, as Supp. Fig. 2f and Supp. Fig. 2j indicate, the system remembers whether a field polarized state has been reached. For Sample#1 (Supp. Fig. 2f), the second (orange) and third (red) up-field ramp curves overlap, and the hysteresis region is much reduced to 5.5 T $< \mathbf{B}_{\parallel armchair} < 6.5$ T. For Sample#2 (Supp. Fig. 2j), the second and third up-field ramp curves also overlap. The hysteresis region is altered compared to the first up-field ramp but is still very large. This sample dependent feature should not be intrinsic but related to details like defects and imperfections in each crystal.

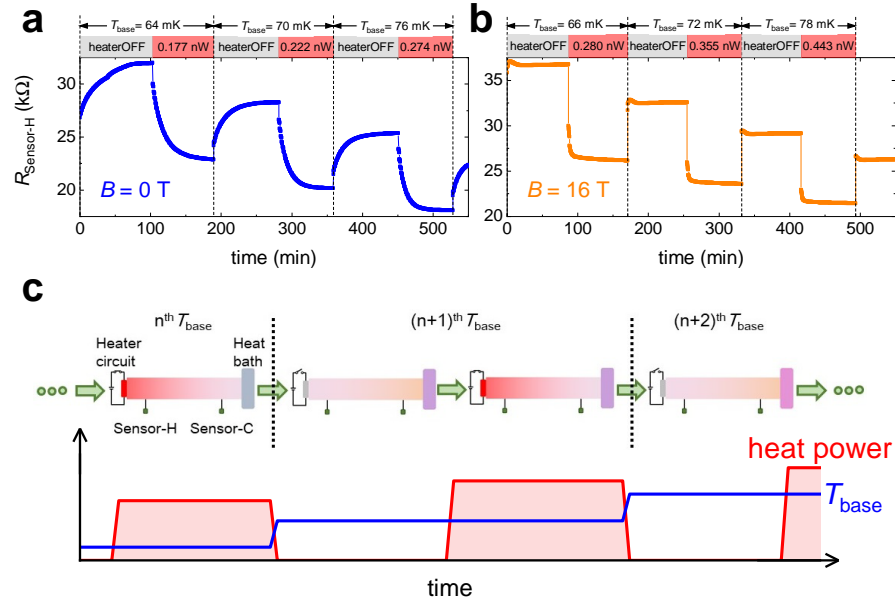
Scenario B: NCTO in the field range of 3 T $< \mathbf{B}_{\parallel armchair} < 6.5$ T is characterized by a unique magnetic order, with different domains, *e.g.*, of a canted *zigzag* phase. The system is expected to develop an approximately equal distribution of domains for small fields. The domain boundaries can scatter phonons, if the domain size is not less than the phonon wavelength, estimated to be of the order of $1 \mu\text{m}$ at the relevant temperature range. When

the system re-enter this $3 \text{ T} < \mathbf{B}_{\parallel armchair} < 6.5 \text{ T}$ phase from high field ($\mathbf{B} \parallel armchair$), one of the domains is preferred. As a result, the overall domain boundary is reduced, thus increases κ . Pinning effect helps the system to preserve the unequally populated domains to some extent (in a sample dependent manner) when entering this $3 \text{ T} < \mathbf{B}_{\parallel armchair} < 6.5 \text{ T}$ phase again from the zero-field state.

To distinguish between the two scenarios is beyond the scope of the current paper. For this purpose, a careful field dependent heat capacity (C_p) measurement at very low temperature is desired. Since domain boundaries are thermodynamically trivial, C_p is expected to be hysteretic in the range of $3 \text{ T} < \mathbf{B}_{\parallel armchair} < 6.5 \text{ T}$ for **Scenario A**, while is not expected by **Scenario B**.

Supplementary Note 3: Possible huge heat capacitance in the zero-field phase of NCTO in the low temperature limit.

Our raw data already show some indirect evidences for huge heat capacitance in the zero-field phase of NCTO. As Supplementary Fig. 3 shows, the system needs a very long time to reach thermal equilibrium at zero field, after the system status is changed. When the system is driven to the polarized phase (16 T, for example), the time needed for thermal equilibrium is greatly reduced. Note that in the relevant temperature range (sample temperature less than 100 mK), the thermal conductivity is nearly field independent (See Fig. 1b), so the time needed for achieving a steady-state heat flow can be roughly estimated as a gauge for the heat capacity. Obviously, the larger sample heat capacity, the longer the system needs to reach thermal equilibrium. Taken together, our raw data indeed suggest that the ground state of NCTO at zero field has huge heat capacity, which is greatly reduced in the field polarized state. This indicates a very large DOS of localized magnetic excitations in the zero-field phase.



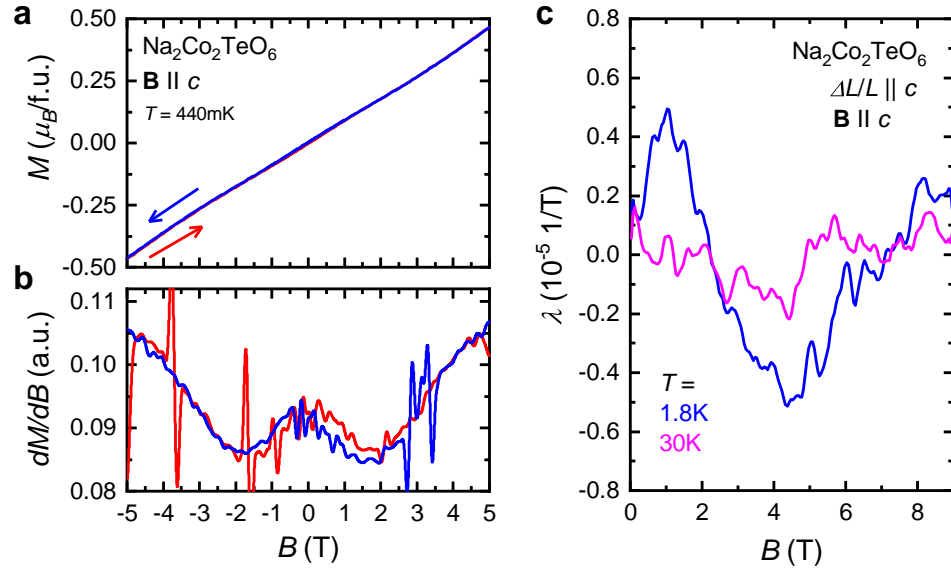
Supplementary Figure 3 | Raw data of a representative thermometer during a typical measurement in different fields. The time profile of the resistance of a thermometer (RX-102 RuO₂ bare chip from Lakeshore Inc.) **a**, at zero field and **b**, at 16 T (in-plane). The measurement was performed in the “self-calibrated” manner, that is to collect the resistance values of the thermometer with sample heater OFF (for calibration) and with sample heater ON (for calculating κ) during the same heating-up process. The base temperature (T_{base}) was kept constant for each step, and the system is left to reach thermal equilibrium until the data were collected. The presented results are collected during the thermal equilibrium process. The sample heater status is indicated by the alternative gray and pink bars. The values in the pink bars are the heating powers generated for each state in the sample heater ON status. **c**, Abridged general view of the experimental setup and procedure. The time profile of T_{base} and power generated by the heater are sketched in the lower panel.

Supplementary Note 4: Thermodynamic properties under fields perpendicular to the honeycomb plane.

Our thermodynamic measurements under out-of-plane magnetic fields found relatively

smooth $M(B)$ curves in the investigated parameter range. However, the field derivative dM/dB highlights their non-linearity. Similarly to the magnetization, the magnetostriction curves also show non-linearity, which points to competing magnetic and elastic energy scales.

As mentioned in the main text, a recent work of thermodynamic measurements performed up to higher magnetic fields found anomalies attributed to phase transitions [31], which match the features of our $\kappa(B)$ isotherms. These anomalies are out of range of the fields reached in Supplementary Fig. 4.



Supplementary Figure 4 | Thermodynamic properties of NCTO under fields

perpendicular to the honeycomb plane. **a**, Magnetic field dependence of the magnetization at 440 mK ($\mathbf{B} \parallel c$). The magnetic field was applied in both $+c$ and $-c$ directions up to 5 T. The field derivative dM/dB is shown in panels **b**, and **c**. Longitudinal magnetostriction measured at 1.8 K and 30 K along the c axis ($\Delta L \parallel c$) with magnetic field applied along the c axis ($\mathbf{B} \parallel c$), too.